Influence of contact interaction character on residual stresses arising over damaged area in composite plate

Vladimir Pisarev, Sviatoslav Eleonsky
Central Aero-Hydrodynamics Institute named after Prof. N.E. Zhukovsky (TsAGI), 1 Zhukovsky Street, Zhukovsky, 140180 Moscow Region, Russian Federation
VSP5335@mail.ru, http://orcid.org/ 0000-0002-5378-609X
juzzepka@mail.ru, http://orcid.org/ 0000-0003-4345-067X

Yury Matvienko
Mechanical Engineering Research Institute of the Russian Academy of Science, 4 Maly Kharitonievsky Pereulok, 101990 Moscow, Russian Federation
ygmatvienko@gmail.com, http://orcid.org/ 0000-0003-2367-0966

Galina Gvozdeva
UAK "Yakovlev" 68, Leningradsky Prospekt, Moscow, 125315, Russian Federation
Galina.Gvozdeva@yakovlev.ru

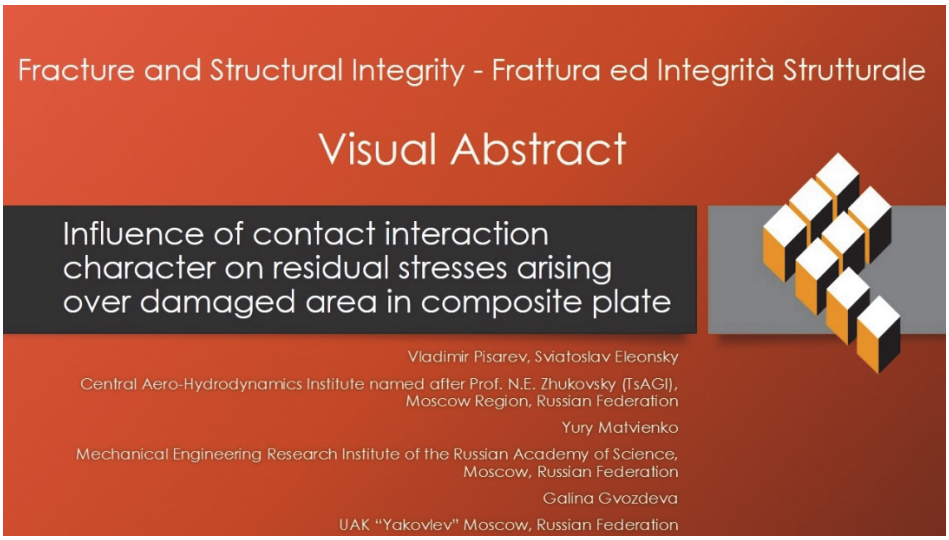

Citation: Pisarev, V., Eleonsky, S., Matvienko, Y., Gvosdeva, G., Influence of contact interaction character on residual stresses arising over damaged area in composite plate, Fracture and Structural Integrity, 73 (2025) 108-130.

Received: 17.03.2025
Accepted: 12.05.2025
Published: 13.05.2025
Issue: 07.2025

KEYWORDS. Composite materials, Contact interaction, Impact damage, Residual stresses. Hole drilling method, Speckle-pattern interferometry

INTRODUCTION

References included in previous paper [1] describe in sufficient detail the relevance and importance of experimental studies related to the assessment of the impact damage on the residual strength of composite structures, which are made from carbon fibre reinforced polymers (CFRP). In the same place, a new approach to the selection of a design

parameter, which can be used for a direct relationship between the impact energy and the damage degree of the composite material, is proposed and implemented.

To date, a wide range of non-destructive methods have been used to characterize the external shape and internal structure of defects in composite materials [2–3]. Over the past six years, a number of papers have appeared, in which various parameters connected with impact damages of composite materials are determined based on advanced experimental methods. These techniques are: ultrasound, computed tomography, infrared thermography, high-speed optical imaging, and shearography [4-10]. The data obtained is then used to assess the residual strength of various composite structures [11-19]. The common feature of all above-mentioned techniques resides in the fact that measurement output consists of undirect parameters, such as a number of transverse matrix cracks, degree of delamination through the thickness of impacted specimens, as well as a level of fiber breakages. This fact means that non-destructive methods are not capable to provide quantitative parameters, which can be reliably used as design criteria for impact resistance of composite materials of any stacking sequence. Obtained data cannot be used for reliable prediction of residual strength. Experimental information, required for this procedure, is not available.

Previously obtained data clearly evidence that residual stresses inherent in contact interaction area can be reliably used as design criteria for impact resistance of composite materials [1]. These criteria are essential to establish a correlation between the results of residual strength tests of damaged structures and the quantitative characteristics of the residual stress field caused by an impact influence. Quantitative data related to residual stress values and distributions over contact interaction zone might be used, firstly, as reliable indicator of damage level and area. Secondary, such information is the link essential for numerical simulation of damaged composite structures and further prediction of both static strength and durability. To confirm the reality of the above statements, it is necessary to increase the amount of data related to the effect of contact interaction parameters on the residual stress values in the damaged area.

The paper presents new data that quantify the effect of the thickness of samples with longitudinally-transversely stacked layers and the impact energy on the residual stresses in the contact interaction zone. Contact dimples arise after both slaw indentation of steel ball of 16 mm diameter and dynamic impact by steel impactor with hemispherical tip of 20 mm and 25 mm diameter. The experimental approach is based on drilling probe holes and subsequent measurements of the local deformation response using the electronic speckle-pattern interferometry (ESPI) method [21-22]. The problem of the first priority consists of obtaining high-quality interference fringe patterns generated by residual stress energy release due to local material removal, which are capable of providing reliable acquisition of initial experimental data. This problem has been successfully overcome for the studied samples. On this base the values of residual stresses that occur with the same parameters of static indentation of a steel sphere of the same diameter into samples with the same layer arrangement, but of different thicknesses, are compared. The values of residual stresses corresponding to the same impact energy but different diameters of the hemisphere of the impact instrument are also analyzed. All residual stress values inherent in damaged area of composite coupons are obtained for the first time.

This paper is only the second publication devoted to the quantitative determination of residual stresses that occur in the area of impact damage to composite structures. The global trend over the past 20 years has been aimed at the technical improvement of non-destructive testing methods for characterization of contact damage of composite materials. This process has brought certain achievements. In particular, the effectiveness of methods based on computed/infrared tomography has significantly increased, which made it possible to visualize impact damage throughout the thickness of composite coupons. Despite this, reliable quantitative criteria have not yet been obtained that make it possible to link residual strength with impact energy for composite structures of different thicknesses with different stacking sequences. There is every reason to believe that the results of determining the values and distributions of the residual stresses components in samples of different thicknesses and different impact energies obtained in this work using a destructive approach have significant potential to create the necessary criteria.

OBJECTS OF INVESTIGATIONS

The powerfulness of the developed approach by using CRFP coupons of cross-ply stacking sequence $[0/90/]_{6S}$ and dimensions of 180×30×4.8 mm has been firstly demonstrated in work [1]. Present paper concerns enlarging data collection by obtaining residual stress values for more thick specimens of the same stacking sequence and plane dimensions. The elements of this collection include, firstly, the magnitudes and distributions of the principal residual stress components, which are obtained, as in a thin sample, by static indentation of a steel sphere with a diameter of 16 mm with a force of 3.0 kN. Secondly, data were obtained on the values and distributions of the principal residual stress components

in the vicinity of the contact dimple, which is caused by an impact damage with an energy of 55 J and an indenter with an outer hemisphere diameter of 20 mm. The previous results for a 20 mm impactor were obtained at an impact energy of 40 J for a 4.8 mm thick coupon [1]. Thirdly, the values and distributions of residual stresses corresponding to the impact damage of a sample of 6.4 mm thick by an impactor with a hemisphere diameter of 25 mm and an impact energy of 55 J are obtained.

To obtain the above-declared results, three specimens of dimensions 180×30×6.4 mm having cross-ply stacking sequence $[0/90/]_{6S}$, which are manufactured from carbon fibre reinforced polymer (CFRP), serve as the objects of investigations. All coupons are cut from a single initial blank with dimensions in plane of 320 x 320 mm using a milling process. Generalized elastic properties of orthotropic composite plates are: Longitudinal modulus E_1 = 73.1 GPa; Transverse modulus. E_2 = 73.1 GPa; Shear modulus G_{12} = 5.3 GPa; Poisson's ratio $\nu_{12} = \nu_{21} =$ 0.25. These characteristics follow from the results of impact-induced vibration mode analysis as it is described in work [21].

All samples contain a pair of contact dimples, each of which is located at 65 mm distance from end face of all specimens as it is shown in Fig. 1. The slow indentation of a hardened steel ball with a diameter of 16 mm serves to realize the static case (CP_S coupon). Two other coupons are undergone to impact influence through the use of a Instron/Dynatup 9250HV drop weight impact testing machine. Impact damages were inflicted according to the standard ASTM methodology (ASTM D7137–17 Standard) with an impactor mass of 15 kg and a hemispherical tip 20 mm (CP_D-20 coupon) and 25 mm (CP_D-25 coupon) in diameter. The test specimens were rigidly clamped in a horizontal position on a massive steel plate located at the bottom of the vertical tower of impact drop tower. The designations of the samples, the magnitude of the external static pressure and the values of the impact energy are listed in Tab. 1.

Sample	External load P, kN	Energy of impact E, J	Diameter of contact dimple $2R_0$, mm
CP_S	3.0		6.0
CP_D-20		55	6.4
CP_D-25		55	8.2

Table 1: Designation of samples, static pressure load and conditions of contact interaction.

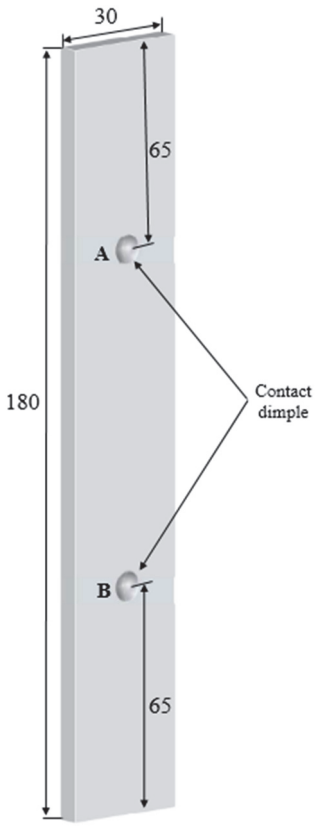

Figure 1: Location of two contact dimples on the coupon's face.

Mutual location of contact dimple borders and probe hole contours is shown in Fig. 2, 3 and 4. Fig. 2b depicts local coordinate system used (y –axis coincides with the vertical symmetry axis of each individual probe hole). Through holes, essential for residual stress deriving, are of 2.0 mm diameter. Hole number increase corresponds to the drilling order. The impact of 20 mm hemispherical tip (CP_D-20 coupon) leads to revealing the image of the dimple contour due to visible surface layers damages as it is shown in Fig. 3a.

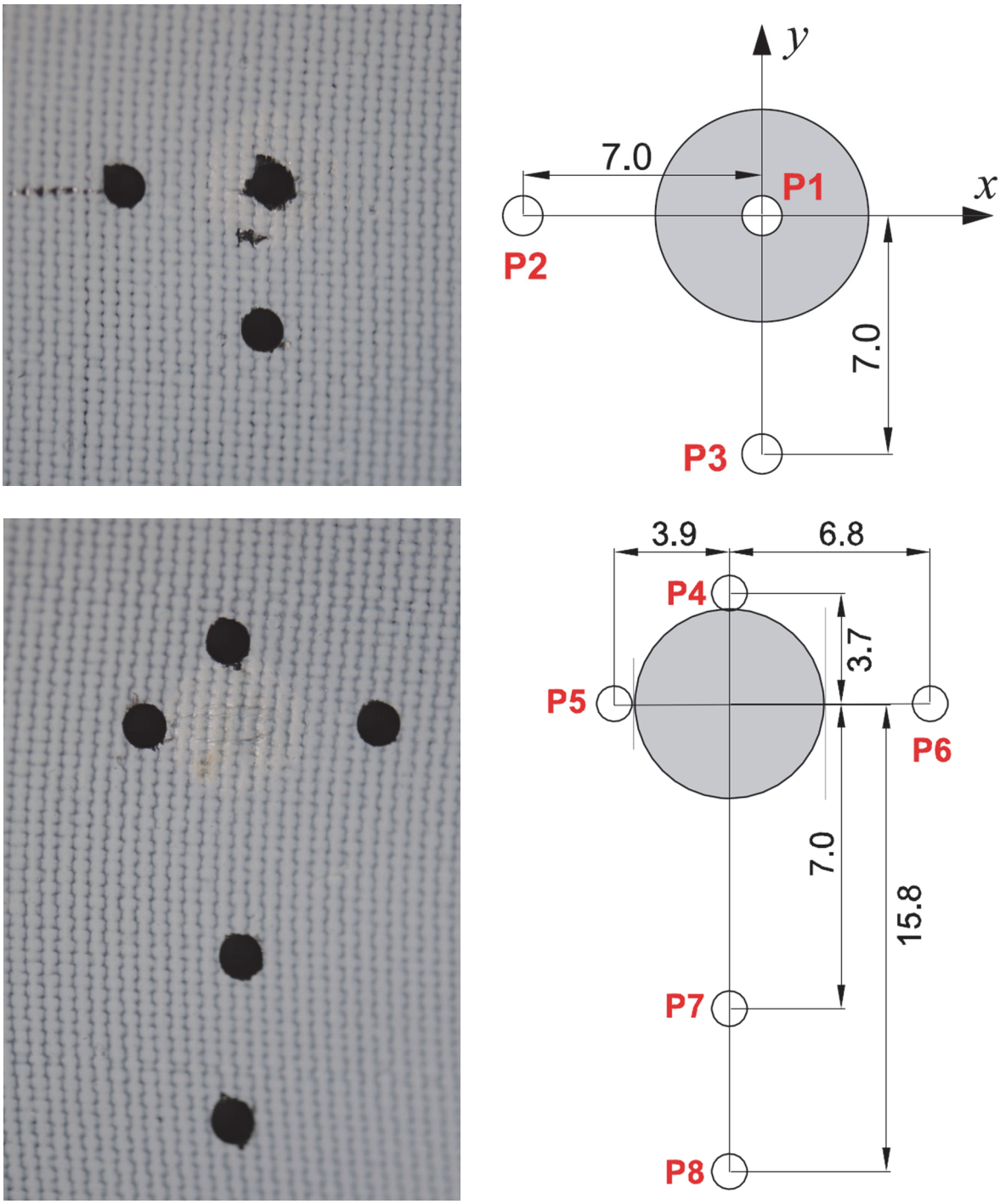

(a) Real image (b) Scheme

Figure 2: Mutual location of contact dimple border and probe hole edges in CP_S coupon.

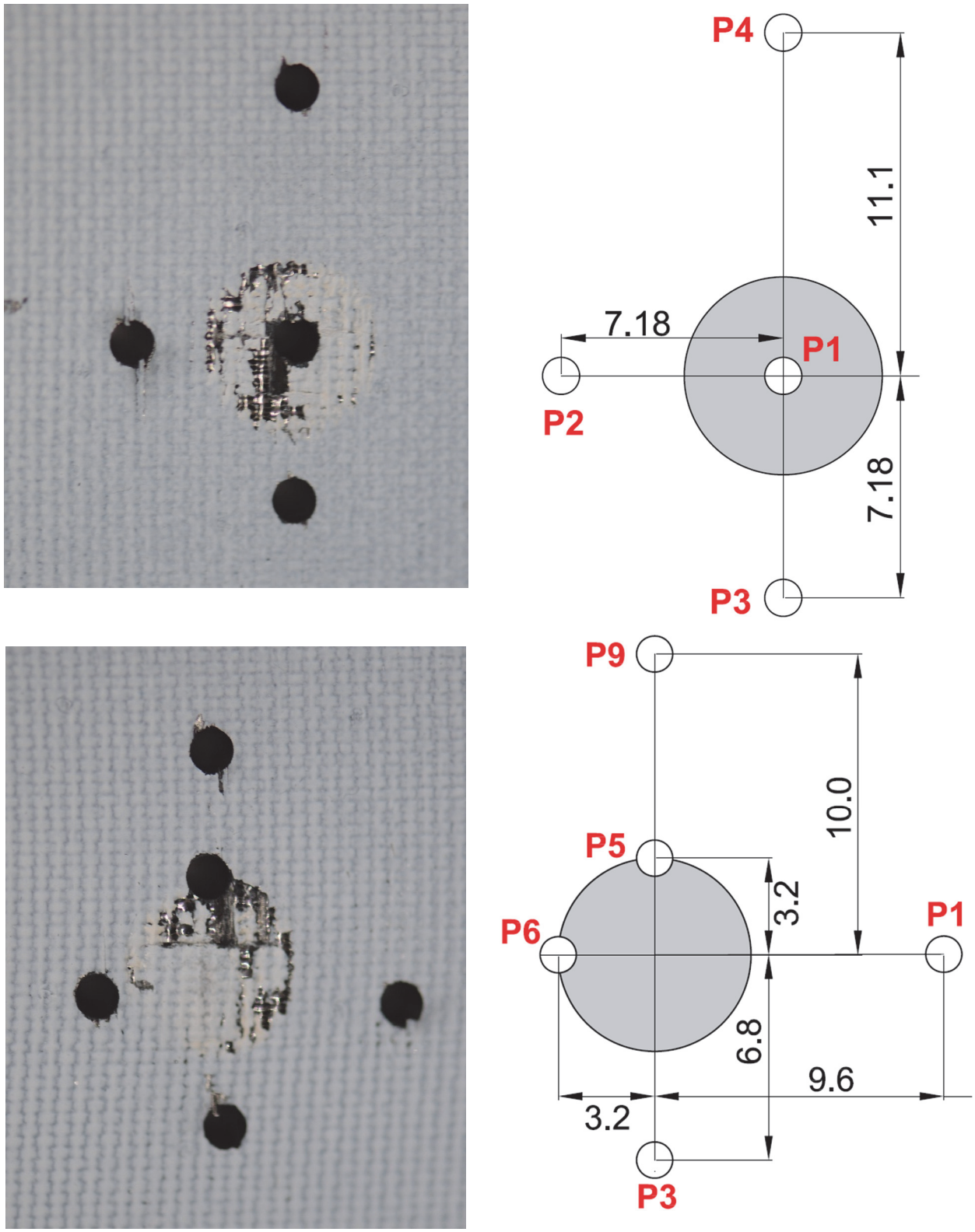

(a) Real image (b) Scheme

Figure 3: Mutual location of contact dimple border and probe hole edges in CP_D-20 coupon.

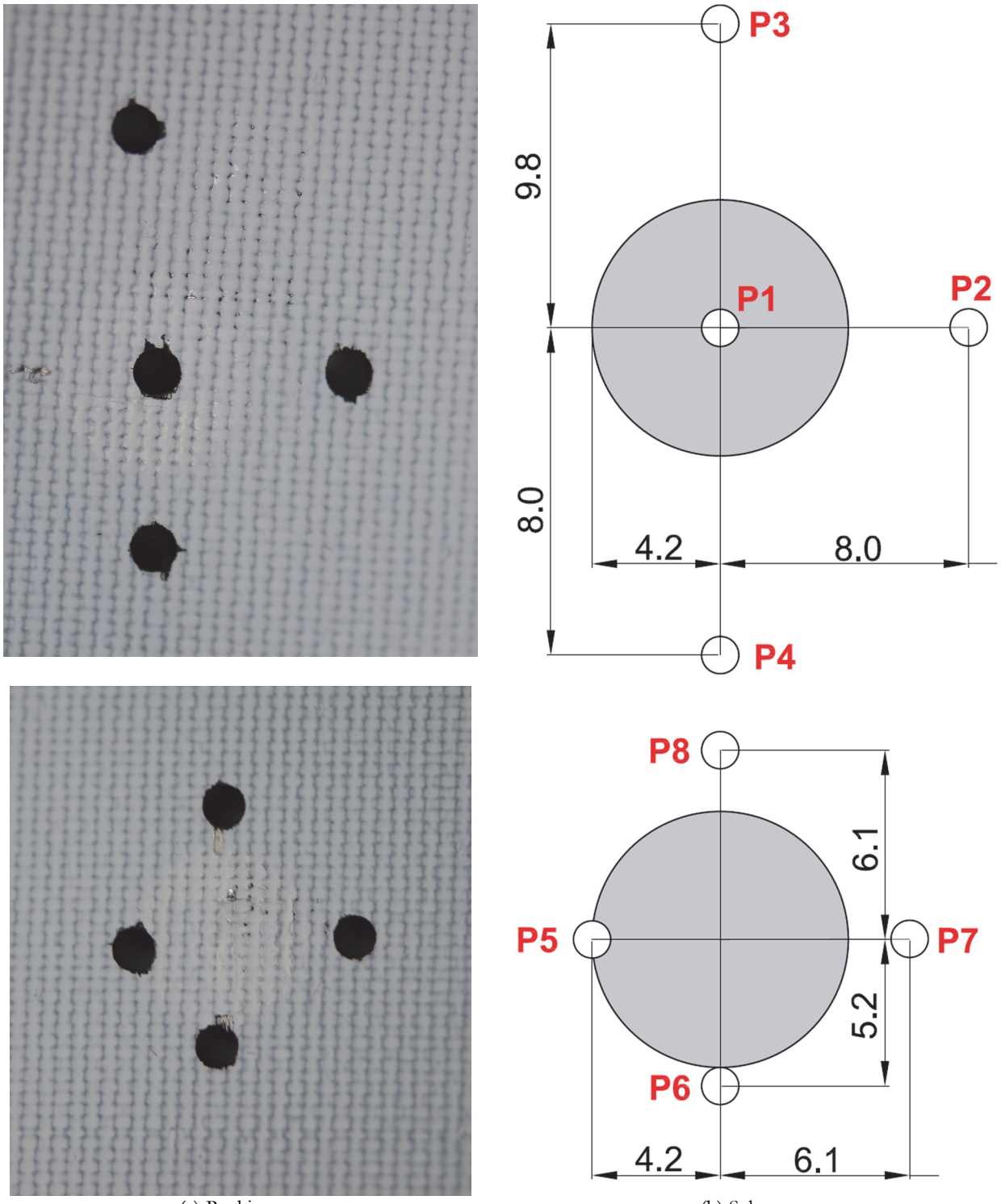

(a) Real image (b) Scheme

Figure 4: Mutual location of contact dimple border and probe hole edges in CP_D-25 coupon.

INITIAL EXPERIMENTAL INFORMATION

Statically induced dimple

Initial experimental information has a form of interference fringe patterns (so-called interferograms or interference images), a source of which is the release of intrinsic energy from residual stresses due to through hole drilling. Obtained interference images reflect distributions of in-plane displacement component *u* (along horizontal direction) and *v* (along

vertical direction) for each individual hole. Detailed description of the experimental procedure is presented in works [20–21]. Interference fringe patterns obtained as a result of probe hole drilling at point 1 of CP-S coupon are shown in Fig. 5. The hole looks slightly blurred due to damage to the surface layers of the material. Nevertheless, this circumstance does not prevent good resolution of interference fringes in the immediate vicinity of its contour.

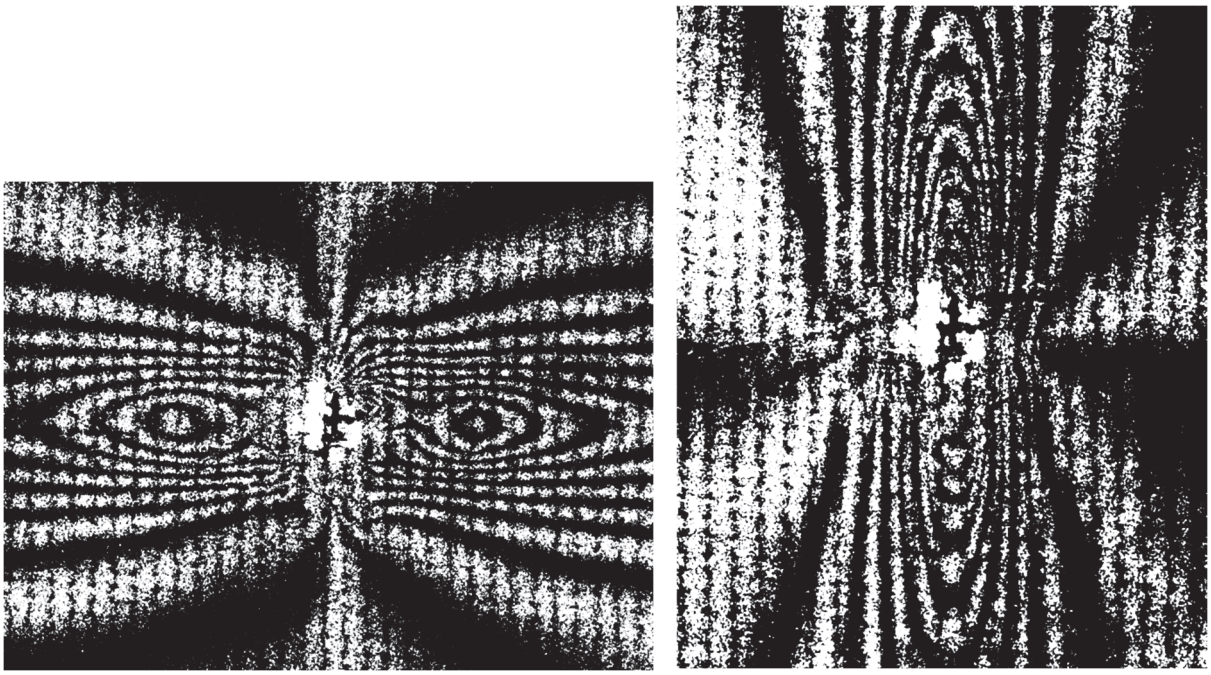

(a) Component u, $\Delta N^{u} = -17.5$ (b) Component v, $\Delta N^{v} = -22.0$

Figure 5: Specimen CP_S. Interferograms referred to point 1.

Interference fringe patterns, visualized at various points in the vicinity of the contact dimple after drilling a through hole, are shown in Fig. 6.

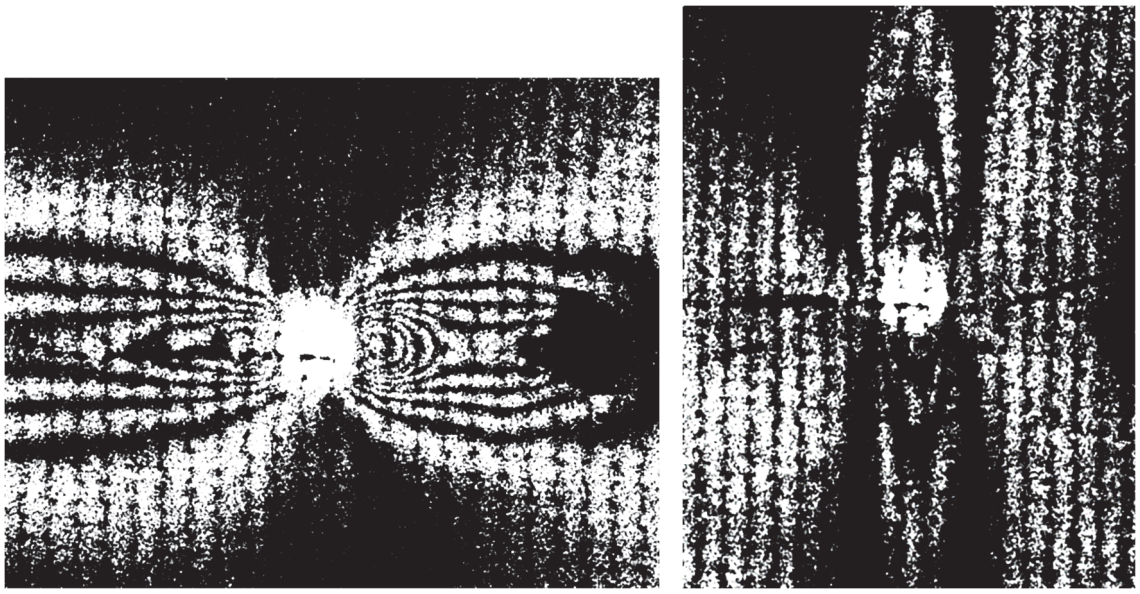

(a) Component u, $\Delta N^{u} = -13.5$ (b) Component v, $\Delta N^{v} = +7.5$

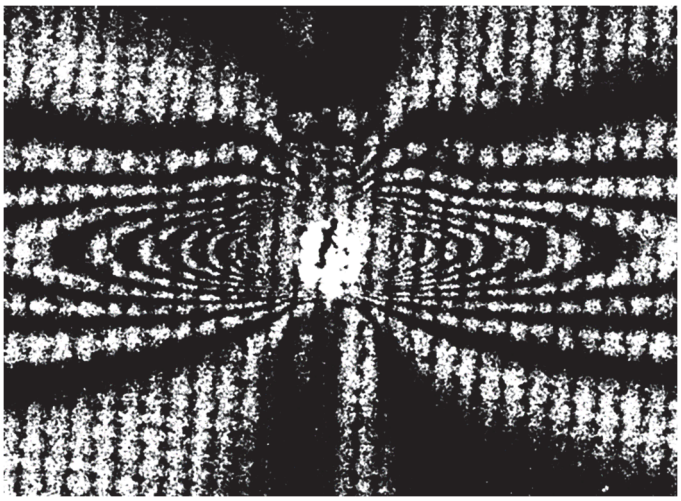

(c) Component u, $\Delta N^{u} = +27.0$

(d) Component v, $\Delta N^{v} = -20.5$

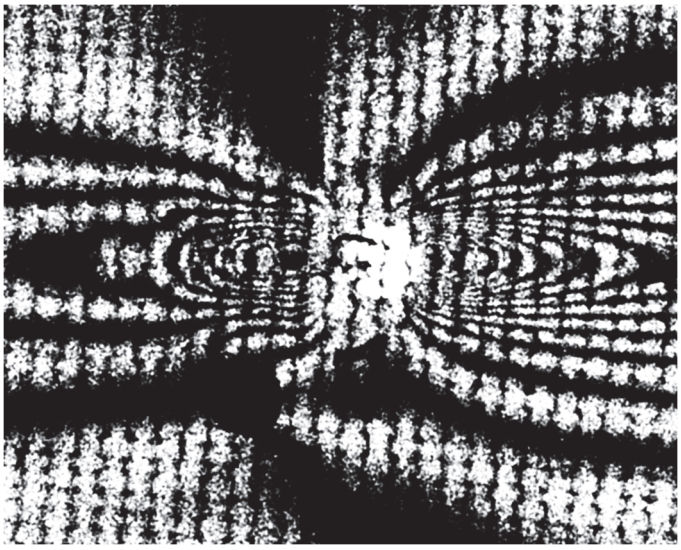

(e) Component u, $\Delta N^{u} = -23.0$

(f) Component v, $\Delta N^{v} = +15.0$

Figure 6: Specimen CP_S. Interferograms referred to point 2 (a), (b); point 4 (c), (d) and point 5 (e), (f).

Interferograms marked by letters (a) and (b), which are obtained for point located relatively far from the dimple edge, demonstrate high quality, which provides reliable resolution of fringes over the hole edge. Interference images, obtained for points 4 (Fig. 6(c, d)) and 5 (Fig. 6(e, f)), reveal quite high quality, which provides reliable resolution of high-density fringes over the hole edge. Centers of probe holes drilled at point 4 and point 5 are located very close to contact dimple border. This is a reason of high-density fringe arising in both horizontal and vertical direction. Maximal value of absolute fringe order difference, which is counted in horizontal direction for point 4, equals to $\Delta N^{u} = +27.0$ fringes. This value, related to the hole of 2.0 mm diameter, is close to the resolution limit of ESPI technique.

Impact dimple induced by hemispherical tip of 20 mm diameter

The size of the hemispherical impactor and the impact energy were chosen so as to obtain a contact dimple with a diameter that is close in magnitude to that of a static indentation of a steel ball with diameter of 16 mm. Interference images visualized after probe hole drilling at point 1 of CP_D-20 coupon are presented in Fig. 7. The quality of the fringes leaves much to be desired, due to the significant degree of damage to the surface layers of the material. Thus, values of absolute fringe order differences can be only approximately counted as it is illustrated in Fig. 7. Note, however, that these differences have a negative physical sign as it takes place in statically induced case (see Fig. 5).

(a) Component u, $\Delta N^{u} \approx -9.0$ (b) Component v, $\Delta N^{v} \approx -14.0$

Figure 7: Specimen CP_D-20. Interferograms referred to point 1.

Interference images, obtained at various points in the vicinity of the contact dimple after drilling a through hole, are shown in Fig. 8

(a) Component u, $\Delta N^{u} = -9.0$ (b) Component v, $\Delta N^{v} = +9.5$

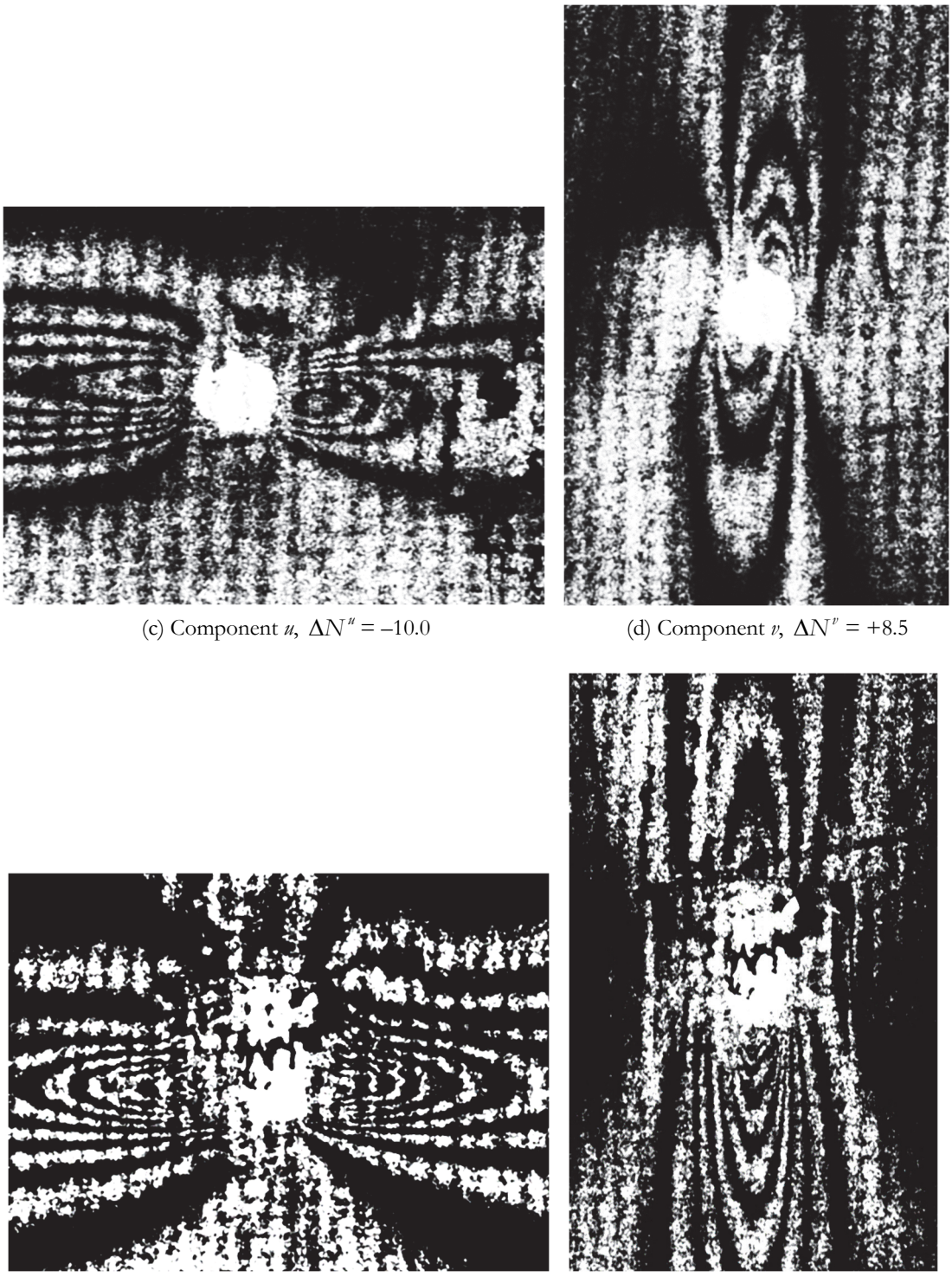

(c) Component u, $\Delta N^{u} = -10.0$ (d) Component v, $\Delta N^{v} = +8.5$

(e) Component u, $\Delta N^{u} = +20.0$ (f) Component v, $\Delta N^{v} = -12.5$

Figure 8: Specimen CP_D-20. Interferograms referred to point 2 (a), (b); point 8 (c), (d) and point 5 (e), (f).

Involved points are located both close to the contour of the dimple and some distance from its boundary. Figs. 8(a, b) and 8(c, d) include interference fringe patterns inherent in point 2 and point 8, respectively, which are located out of contact dimple area. This fact considerably increases the fringe quality comparing with images presented in Fig. 7. The quality of the fringes visualized at point 5 (Fig 8(e, f)) is quite satisfactory for quantitative processing, despite the fact that the probe hole partially overlaps the damaged contour of the contact dimple.

Impact dimple induced by hemispherical tip of 25 mm diameter

There are two ways to reduce the degree of destruction of the surface layers of the composite material and, thereby, ensure reliable obtaining of the values of the principal residual stress components in the center of the contact dimple. The first one is to reduce the energy impact. The second way is to increase the impact surface area at the same energy. In this work, the second approach was chosen, namely, a tool with a hemispherical tip of 12.5 mm radius was used. The images shown in Fig. 4a confirm the correctness of this choice. Interference images visualized after drilling of probe hole at point 1 of CP_D-25 coupon are presented in Fig. 9. Fringe patterns shown in this figure, as opposed to images in Fig. 7, demonstrate a fairly high fringe quality and are quite suitable for a quantitative interpretation in terms of absolute fringe order differences.

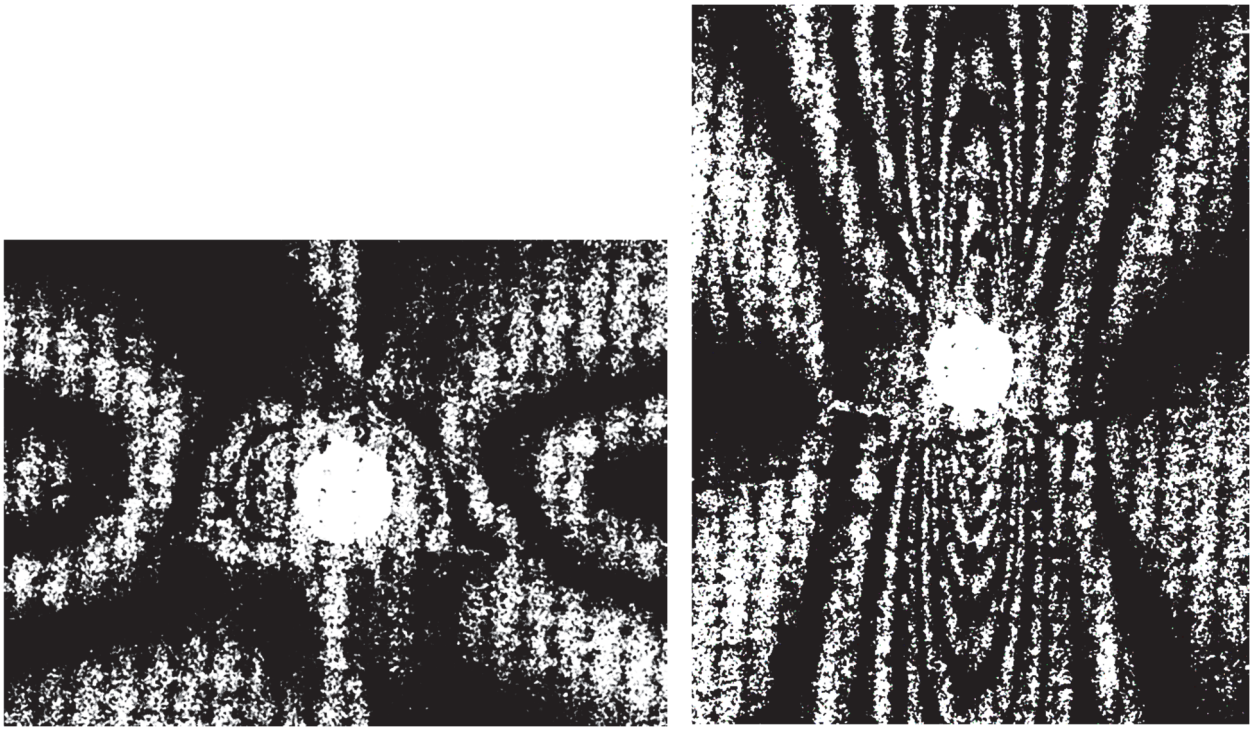

(a) Component u, $\Delta N'' = -5.0$ (b) Component v, $\Delta N'' = -19.5$

Figure 9: Specimen CP_D-25. Interferograms referred to point 1.

Interference fringe patterns, a source of which is deformation response to through hole drilling at the vicinity of contact dimple at point 5 and point 6 caused by impact influence on CP_D-25 coupon, are shown in Fig. 10. These interferograms reveal quite high quality, which provides reliable resolution of high-density fringes over the hole edge. Centers of probe holes drilled at point 5 and point 6 are located very close to contact dimple border. This is a reason of high-density fringes arising in both horizontal (point 6) and vertical (point 5) direction. Maximal value of absolute fringe order difference, which is counted in horizontal direction for point 6, equals to $\Delta N'' = +27.0$ fringes. Note again that this value, related to the hole of 2.0 mm diameter, is close to the resolution limit of ESPI technique.

Interference fringe patterns, a source of which is deformation response to through hole drilling at the vicinity of contact dimple at point 4 and point 7 caused by impact influence on CP_D-25 coupon, are shown in Fig. 11. The fact that probe holes are located out of contact dimple area provides very good fringe quality.

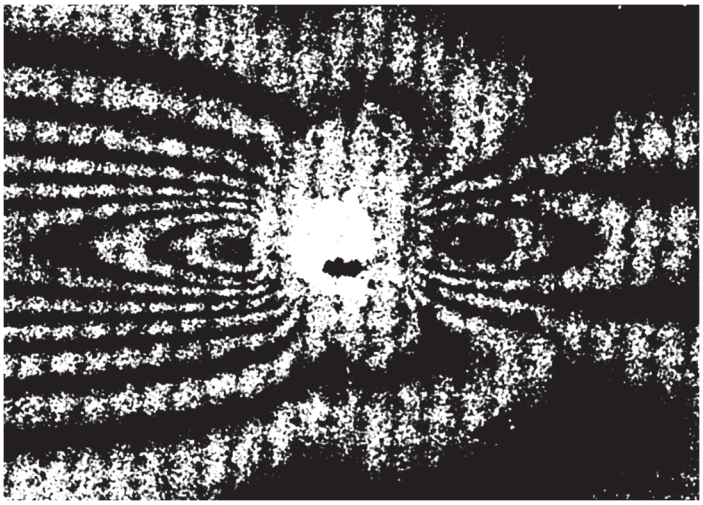

(a) Component u, $\Delta N^{u} = -11.0$

(b) Component v, $\Delta N^{v} = +19.5$

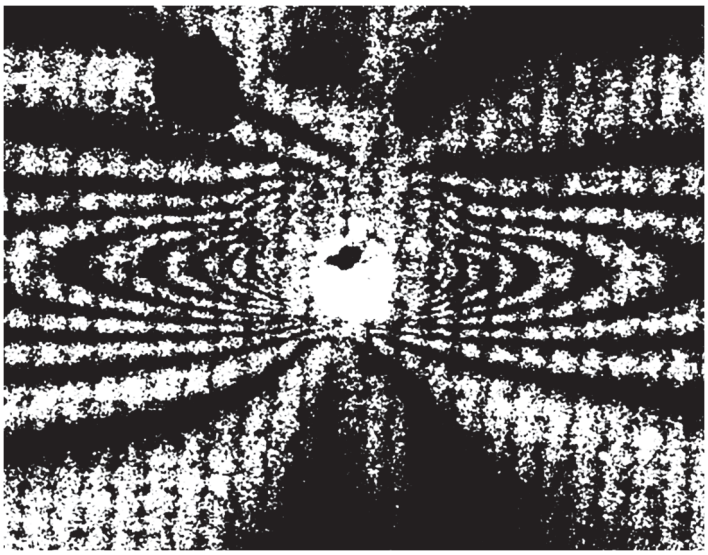

(c) Component u, $\Delta N^{u} = +27.0$

(d) Component v, $\Delta N^{v} = -9.0$

Figure 10: Specimen CP_D-25. Interferograms referred to point 5 (a), (b) and point 6 (c), (d).

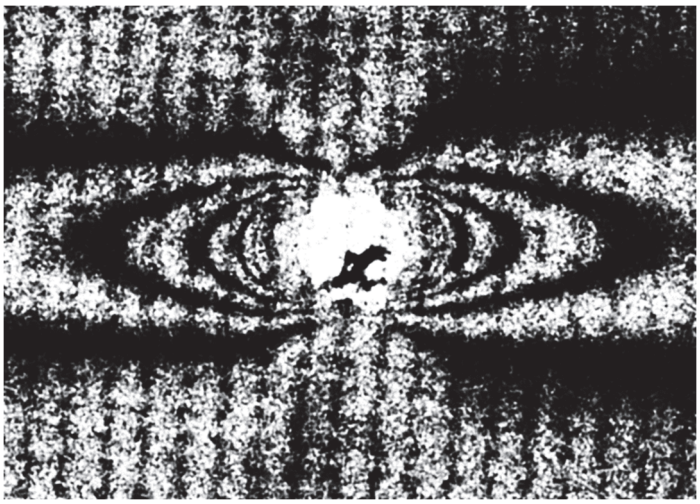

(a) Component u, $\Delta N^{u} = +20.0$

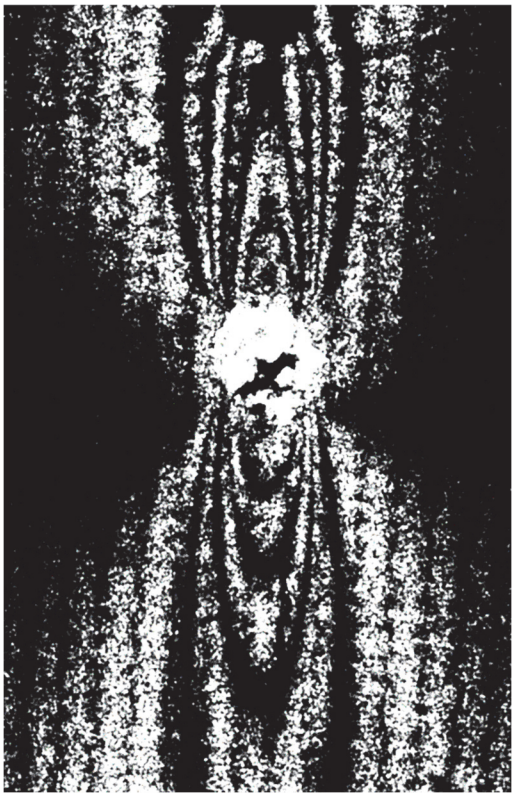

(b) Component v, $\Delta N^{v} = -11.0$

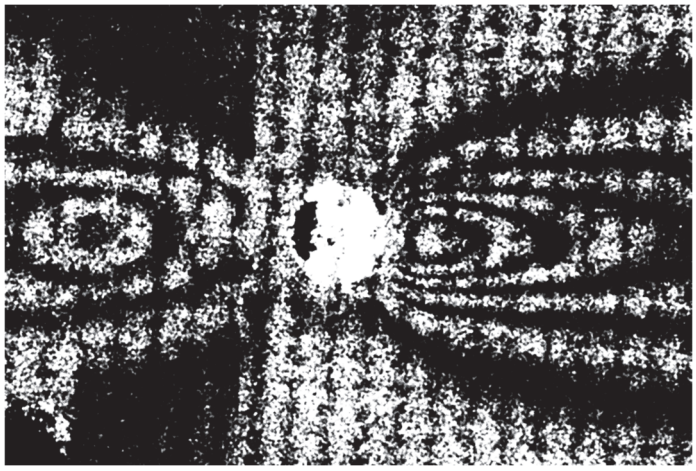

(c) Component u, $\Delta N^{u} = -5.0$

(d) Component v, $\Delta N^{v} = +10.0$

Figure 11: Specimen CP_D-25. Interferograms referred to point 4 (a), (b) and point 7 (c), (d).

Experimental characterization of residual stresses in composite material, which is based on local material removal and subsequent measurements of deformation response by ESPI, always includes technical issue to be addressed. The point is that for carrying out optical interference experiments the initial (black) surface of the coupons must be coated with a thin layer of mat white enamel. Naturally, this fact exerts negative influence on a quality of interference fringe patterns caused by local material removal even though these interferograms are related to undamaged surface area. External surfaces of all coupons are coated by minimally thick paint layer through which the initial cross-ply structure appears. However, most of obtained interference fringe patterns demonstrate a fairly high quality and quite suitable for a quantitative interpretation in terms of fringe order differences. This fact is of great importance from the viewpoint of clarifying the boundaries of the field of application of the developed experimental method. The matter is that previously high-quality interference fringe patterns were obtained for an impact energy of 40 J [1]. The possibility of obtaining interferograms of the same qualitative level for an impact energy of 55 J (27% increase) was completely unobvious until the presented studies have been performed. Visual analysis of interferograms presented in Fig. 5–6 and interference images shown in Fig. 7–11 clearly evidences that two sets of high-quality interferograms, which offer a reliable resolution of interference fringes to quantify hole diameter increments along principal anisotropy directions, have been acquired for both static and dynamic case. This fact, along with the results obtained earlier in work [1], indicates the high reliability and prospects of the developed experimental approach to determining residual stresses in the contact damage zone of composite plates.

DETERMINATION OF PRINCIPAL RESIDUAL STRESS COMPONENTS

The interference fringe patterns shown in Fig. 5–11 have a pronounced symmetrical character with respect to both axes of the local coordinate system (x, y), the origin of which coincides with the centre of each probing hole. Moreover, these axes coincide with the principal axes of anisotropy of the composite material. This fact means that the principal components of the residual stresses σ_1 and σ_2, whose directions coincide with the principal anisotropy axes E_1 and E_2, respectively, can be determined according to the approach described in [1, 20-21]. The values of residual stress components, referred to the middle plane of thin orthotropic plate, can be obtained as:

$$\sigma_1 = \frac{E_1}{2r_0 k}\left\{\frac{n\Delta u + \left(1-\frac{\nu_{12}}{k}\right)\Delta v}{\frac{n^2}{k}-(k-\nu_{12})\left(\frac{1}{k}-\nu_{21}\right)}\right\}, \sigma_1 = \frac{E_2}{2r_0}\left\{\frac{n\Delta v + k^2\left(\frac{1}{k}-\nu_{21}\right)\Delta u}{\frac{n^2}{k}-(k-\nu_{12})\left(\frac{1}{k}-\nu_{21}\right)}\right\}, \quad (1)$$

where σ_1 is directed along the first principal anisotropy axes that coincides with the direction of the greater elasticity modulus E_1; σ_2 is directed along the second principal anisotropy axes that coincides with the direction of the lesser elasticity modulus E_2; r_0 denotes through hole radius; $k = \sqrt{\frac{E_1}{E_2}}$, $n = \sqrt{2(k+1)}$; Δu and Δv are the increments of real hole of 2 r_0 diameter caused by residual stress release in principal anisotropy directions E_1 and E_2, respectively.

All coupons are made from layered fiber-reinforced material with cross-ply stacking sequence. The thickness of each coupon is equal to t = 6.40 mm. Generalized mechanical characteristics of orthotropic composite plates are: Longitudinal modulus E_1 = 73.1 GPa; Transverse modulus. E_2 = 73.1 GPa; Shear modulus G_{12} = 5.3 GPa; Poisson's ratio $\nu_{12} = \nu_{21}$ = 0.25; k = 1; n = 2. Impact-induced vibration mode analysis is implemented for a determination of generalized mechanical properties of orthotropic material. Details of the technique involved are presented in work [21].

Values of hole diameter increment Δu and Δv in principal stress directions, which are essential for residual stress determination, follow from the relations inherent in speckle-pattern interferometry method [22]:

$$\Delta u = \Delta N^u \frac{\lambda}{2sin\Psi}, \ \Delta v = \Delta N^v \frac{\lambda}{2sin\Psi} \quad (2)$$

where $\lambda = 532$ nm is the wavelength of laser illumination; $\Psi = \pi / 4$ is the angle between inclined illumination and normal observation directions; ΔN^{u} and ΔN^{v} represent differences in absolute fringe orders counted over the solitary fringe pattern between two basic points corresponding to the directions of principal stresses σ_1 and σ_2, respectively. Two basic points corresponding to each fringe pattern are defined as the intersection points of the hole diameter coinciding with a specific principal stress direction and the edge of the probe hole. The horizontal and vertical diameters are related to the ΔN^{u} (σ_1-direction) and ΔN^{v} (σ_2-direction) absolute fringe order difference, respectively. Illustrations of fringe count way to determine ΔN^{u} and ΔN^{v} parameters as well as identification procedure of physical sign of in-plane displacement components are thoroughly presented in works [20, 23].

Initial experimental data extracted from the fringe patterns and the calculated values of the principal residual stress components, which are obtained using formulae (1) and relations (2), are listed in Tab. 2, Tab. 3 and Tab.4 for specimen CP_S, CP_D-20 and CP_D-25, respectively.

Point/ Dimple	Distance from dimple center to probe hole center x/y, mm	ΔN^{u}, fringes	ΔN^{v}, fringes	Δu, μm	Δv, μm	σ_1, MPa	σ_2, MPa
1/A	$x_1 = 0,\ y_1 = 0$	–17.5	–22.0	–6.65	–8.36	**–208.2**	**–230.9**
2/A	$x_2 = 7.0,\ y_2 = 0$	–13.5	+7.5	–5.13	+2.85	**–86.4**	**+18.5**
3/A	$x_3 = 0,\ y_3 = 7.0$	+10.0	–13.0	+3.80	–4.94	**+41.4**	**–70.3**
4/B	$x_4 = 0,\ y_4 = 3.7$	+27.0	–20.5	+10.26	–7.79	**+146.8**	**–77.9**
5/B	$x_5 = 3.9,\ y_5 = 0$	–23.0	+15.0	–7.03	+3.04	**–140.4**	**+51.6**
6/B	$x_6 = 6.8,\ y_6 = 0$	–18.5	+8.0	–2.85	+2.85	**–125.3**	**+5.9**
7/B	$x_7 = 0,\ y_7 = 10.3$	+10.0	–12.0	+3.80	–4.56	**+44.4**	**–65.6**
8/B	$x_8 = 0,\ y_8 = 15.8$	+10.0	–4.0	+3.80	–1.52	**+68.7**	**–2.0**

Table 2: The results of fringe patterns interpretation and values of principal residual stress components near contact dimple in CP_S coupon.

Point/ Dimple	Distance from dimple center to probe hole center x/y, mm	ΔN^{u}, fringes	ΔN^{v}, fringes	Δu, μm	Δv, μm	σ_1, MPa	σ_2, MPa
1	$x_1 = y_1 = 0$	–9.0	–14.0	–3.42	–5.32	**–115.5**	**–140.6**
6	$x_6 = 4.2,\ y_6 = 0$	–8.0	+12.5	–3.04	+4.75	**–26.8**	**+76.8**
2	$x_2 = 7.2,\ y_2 = 0$	–9.0	+9.5	–3.42	+3.61	**–43.9**	**+49.5**
8	$x_8 = 9.6,\ y_8 = 0$	–10.0	+8.5	–3.80	+3.23	**–55.1**	**+38.4**
5	$x_5 = 0,\ y_5 = 3.8$	+20.0	–12.5	+7.60	–4.75	**+123.8**	**–40.5**
7	$x_7 = 0,\ y_7 = 6.8$	+13.5	–12.5	+5.13	–4.75	**+71.3**	**–60.1**
3	$x_3 = 0,\ y_3 = 7.2$	+17.0	–9.5	+6.46	–3.61	**+108.6**	**–25.2**
4	$x_4 = 0,\ y_4 = 11.1$	+12.5	–10.5	+4.75	–3.99	**+69.2**	**–47.2**
9	$x_9 = 0,\ y_9 = 10.0$	+14.0	–6.0	+5.32	–2.26	**+92.9**	**–6.8**
(3+7)/2	$x_{(3+7)/2} = 0,$ $y_{(3+7)/2} = 7.0$	–	–	–	–	**+90.0**	**–42.7**
(4+9)/2	$x_{(4+9)/2} = 0,$ $y_{(4+9)/2} = 10.5$	–	–	–	–	**+81.1**	**–27.0**

Table 3: The results of fringe patterns interpretation and values of principal residual stress components near contact dimple in CP_D-20 coupon.

Point/ Dimple	Distance from dimple center to probe hole center x/y, mm	ΔN^u, fringes	ΔN^v, fringes	Δu, μm	Δv, μm	σ_1, MPa	σ_2, MPa
1	$x_1 = y_1 = 0$	–5.0	–19.5	–1.90	–7.41	**–99.6**	**–173.0**
5	$x_5 = 4.2,\ y_5 = 0$	–11.0	+19.5	–4.18	+7.41	**–30.0**	**+124.3**
7	$x_7 = 6.1,\ y_7 = 0$	–5.0	+10.5	–1.90	+3.80	**–10.1**	**+65.7**
2	$x_2 = 8.0,\ y_2 = 0$	0.0	+5.5	0.0	+2.08	**+16.6**	**+44.3**
6	$x_6 = 0,\ y_6 = 5.2$	+27.0	–9.9	+10.26	–3.42	**+191.0**	**+9.1**
8	$x_8 = 0,\ y_8 = 6.8$	+27.0	–12.0	+10.26	–4.56	**+181.9**	**–15.2**
4	$x_4 = 0,\ y_4 = 7.2$	+20.0	–11.0	+7.60	–4.18	**+128.4**	**–28.3**
3	$x_3 = 0,\ y_3 = 9.8$	+13.5	–7.5	+5.13	–4.18	**+86.4**	**–19.7**

Table 4: The results of fringe patterns interpretation and values of principal residual stress components near contact dimple in CP_D-25 coupon.

Data collections, presented in Tab. 2, Tab. 3 and Tab. 4, provide a possibility of constructing distributions of principal residual stress components over horizontal and vertical cross-section referred to the dimple center. To do this experimental information, obtained for two dimples in each coupon, has to be involved thus minimizing a degree of interaction between neighboring probe holes and its influence on the final result. Properly arranged data, extracted from Tab. 2, Tab. 3 and Tab. 4, allow us to construct dependencies of the values of principal residual stress components from the dimple center distance in two orthogonal directions, which are presented in Figs. 12–14.

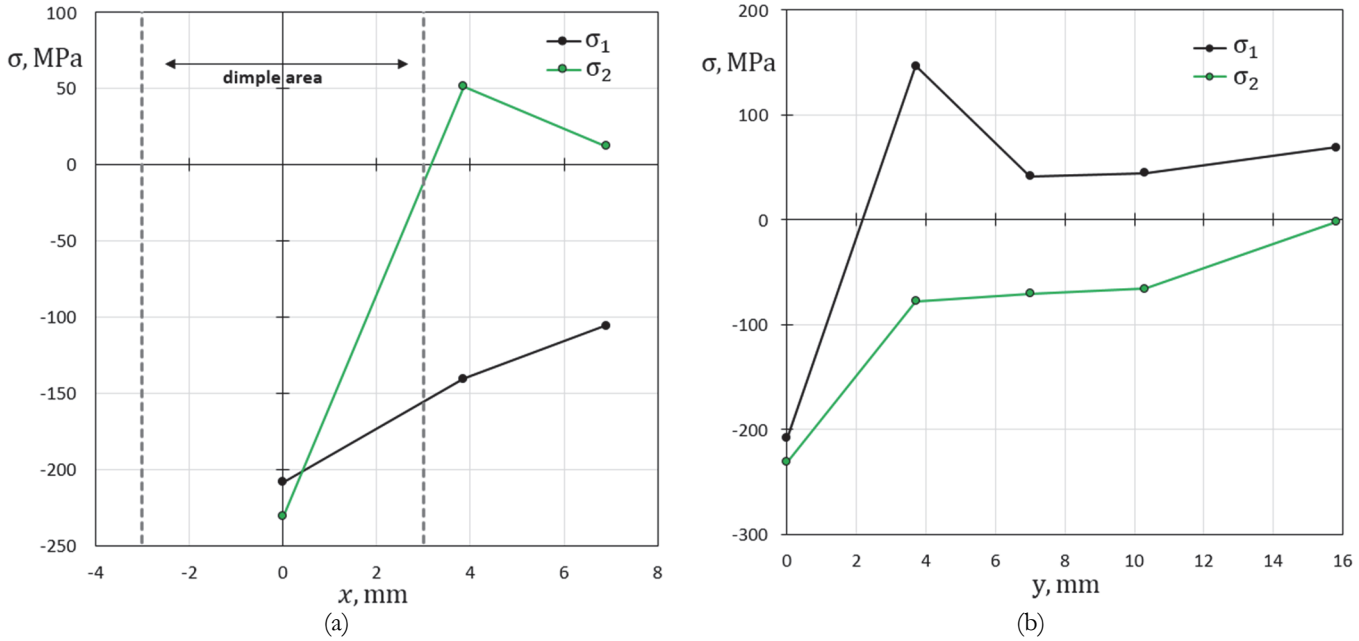

Figure 12: The principal residual stress components σ_1 and σ_2 along horizontal symmetry axis $y = 0$ (a) and vertical symmetry axis $x = 0$ (b) of CP_S specimen as functions of distance from the dimple center.

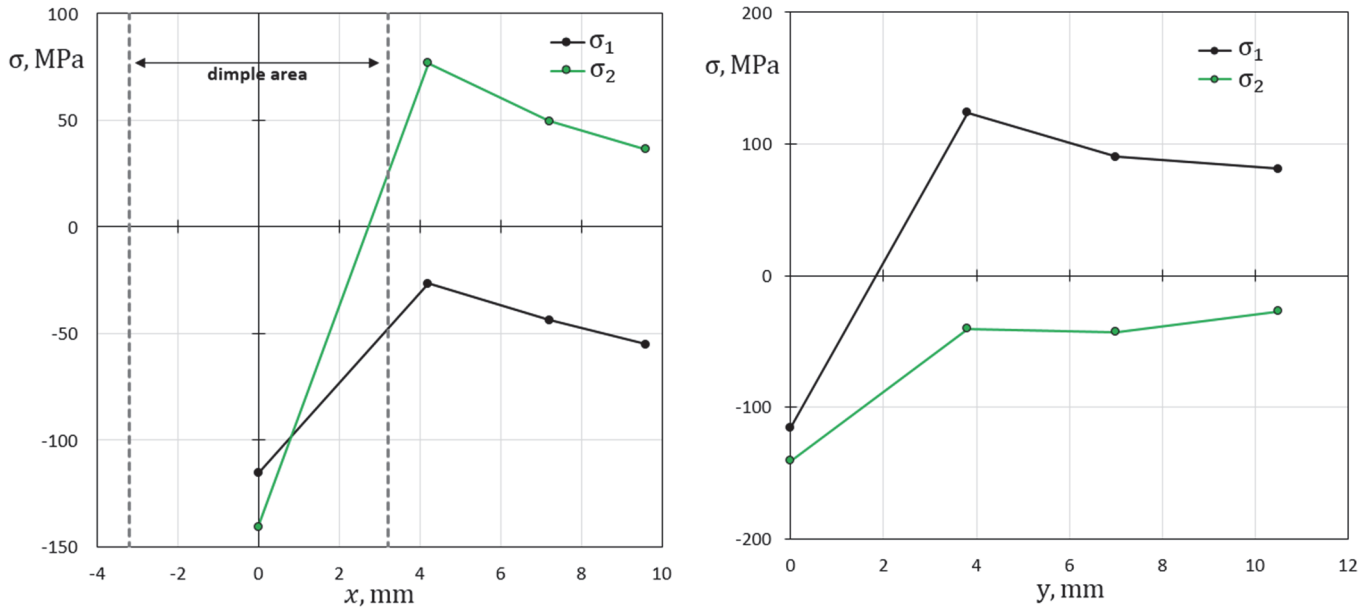

Figure 13: The principal residual stress components σ_1 and σ_2 along horizontal symmetry axis $y = 0$ (a) and vertical symmetry axis $x = 0$ (b) of CP_D-20 specimen as functions of distance from the dimple center.

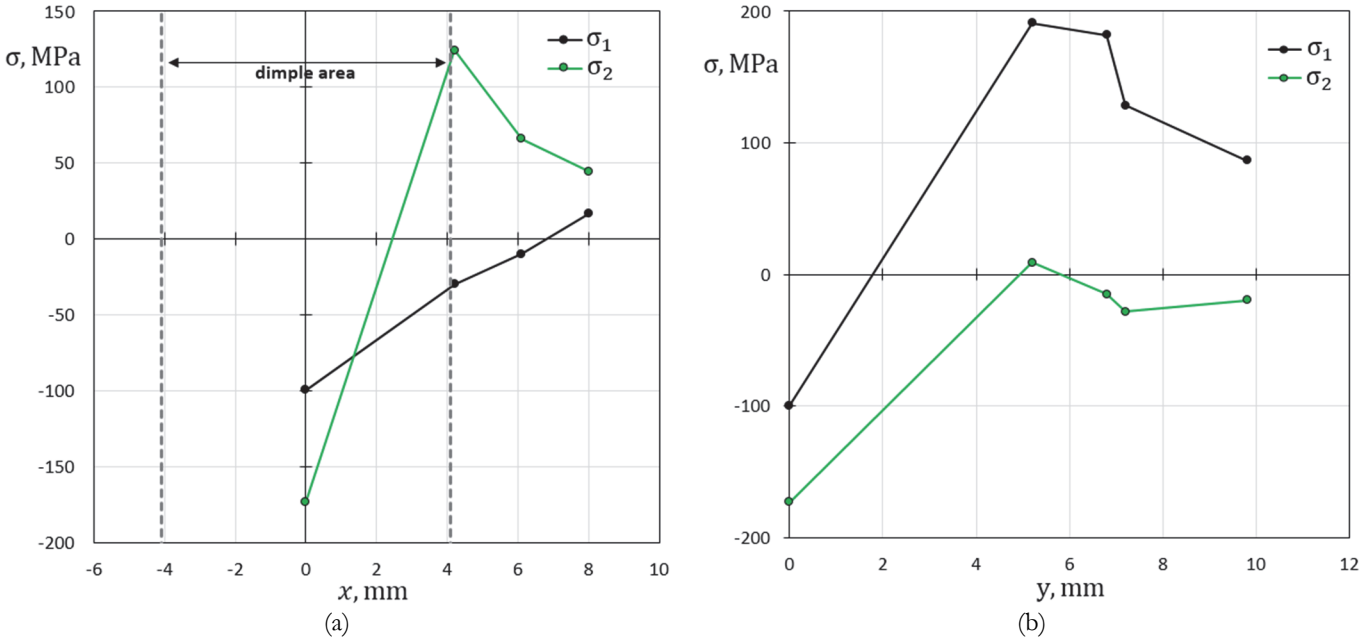

Figure 14: The principal residual stress components σ_1 and σ_2 along horizontal symmetry axis $y = 0$ (a) and vertical symmetry axis $x = 0$ (b) of CP_D-25 specimen as functions of distance from the dimple center.

ANALYSIS OF THE RESULTS

Consideration of the results obtained should begin by answering the question for what purpose the case of static indentation is being investigated. Indeed, the effect of this kind of contact interaction on the residual strength of damaged composite structures is practically not analyzed. However, the chosen two-step procedure is necessary from a methodological point of view. The point is that the possibility of obtaining interference fringe patterns, the quality of which is high enough for reliable quantitative processing, when drilling a hole in the contact interaction zone located in the surface of a composite plate painted with a thin layer of white matte enamel, was completely unobvious. For this reason,

starting experiments in case of impact damage would be a very risky step. That is why reliable visualization of high-quality interferograms in static contact interaction zone is the essential link in the course of undertaken investigations.

It should be firstly noted that coupons, considered in present paper, already contain technological residual stresses [21]. The values of these stresses, obtained by averaging the results of 10 measurement points, equal to σ_1 = +13.9 MPa; σ_2 = + 48.6 MPa. The consequence of initial internal stresses availability is that the character of residual stress distributions along the dimple contour in relation to its center does not have perfect radial symmetrical configuration.

The tangential with respect to the dimple contour residual stress component is tensile stress both for static indentation (CP_S, point 4 – σ_2 = +146.8 MPa; point 5 – σ_2 = +51.6 MPa), and impact influence (CP_D-20, point 5 – σ_2 = +123.8 MPa; point 6 – σ_1 = +76.8 MPa; CP_D-25, point 6 – σ_1 = +191.0 MPa; point 8 – σ_1 = +181.9 MPa; point 5 – σ_2 = +124.3 MPa). Radial components along the dimple edge are compressive stresses for static indentation (CP_S, point 5 – σ_1 = –140.4 MPa; point 4 – σ_2 = –77.9 MPa) and dynamic influence in CP_D-25 coupon (point 6 – σ_1 = –26.8 MPa; point 5 – σ_2 = –40.5 MPa). More complex situation takes place for impact damage in CP_D-25 coupon, namely, σ_1 = –30.0 MPa at point 5 and σ_2 = +9.1 MPa at point 6. The last value is explained by superposition of radial compressive stress component arising due to impact and tensile residual stress component σ_2 = + 48.6 MPa initially existing in the specimen material.

In the following considerations, it is assumed that the tests of damaged samples will be carried out under uniaxial either tension or compression, and the direction of the applied load coincides with the vertical symmetry axis. Firstly, it is necessary to pay attention to the level of σ_2 tensile residual stress component at the point of intersection of the contact dimple contour and horizontal cross-section in CP_D-25 coupon. This value is equal to σ_2 = +123.8 MPa. The fact is that the static strength of the coupons without damage during tensile tests is characterized by ultimate stress σ_B = 750↔800 MPa. Thus, the value σ_2 = +123.8 MPa equals to 15.5% of the limit value. This circumstance should be took into account, especially for fatigue tests.

The second factor, which undoubtedly negatively affects the residual strength, both in tension and compression, is the transition of the component σ_2 sign from "minus" to "plus", which occurs within the contact dimple, as shown in Fig. 12, 13 and 14. It is important to note that such a transition is accompanied by the presence of a significant stress gradient, and all the parameters of σ_2 component distribution can be described quantitatively.

Residual stress components referred to the dimple center are of special interest. The point is that these parameters in *y*-direction are compressive stress components of considerable value, namely, σ_2 = –230.9 MPa and σ_2 = –173.0 MPa for CP_S and CP_D-25 coupon, respectively. This is an evident explanation of the loss of bearing capacity of dynamically damaged plates during compression tests. A comparison of the residual stress component σ_2-values obtained for static and two impact dimples is shown in Fig. 15.

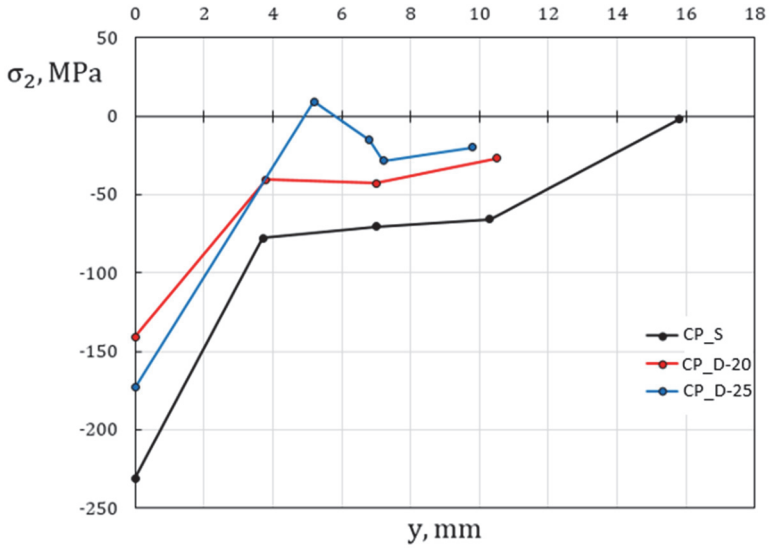

Figure 15: Distributions of principal residual stress component σ_2 for coupons with static and two dynamic contact dimples along vertical symmetry axis x = 0.

The graphs shown in Fig. 15 clearly illustrate the mechanism by which contact damage affects the residual strength of the plates during the most common compression tests. It should be noted that the form of dependencies matches well. The maximum absolute values of the compressive component were obtained for static indentation. However, the nature of the component distributions indicates that with an increase in the impact energy, the same level of residual stresses can be achieved. The question remains to be answered: what is the maximum value of this energy for a specific stalking sequence of the composite material and the thickness of the coupon? The results show that for a hemispherical impactor with a diameter of 20 mm and the impact energy of 55 J, the destruction of the surface fibers of the material makes it difficult to reliably assess the residual stresses in the center of the dimple. However, this procedure can be reliably implemented on the contour of the dimple. When using a hemispherical impactor with a diameter of 25 mm and the impact energy of 55 J, reliable results were obtained both inside and outside the contact dimple. This means that the impact energy can be further increased.

Evaluation of the influence of coupon's thickness as well as an indentation type and parameters on the results of residual stress determination in the vicinity of contact dimple can initially be based on comparative analysis of present data and residual stress distributions obtained in paper [1]. Information, related to static indentation of steel ball of 16 mm diameter in composite plates of different thickness by force $P = 3$ kN, is presented in Tab. 5.

Coupon/ Point	Contact dimple diameter. mm	Distance from dimple center to probe hole center x/y, mm	σ_1, MPa	σ_2, MPa
CP_S /1	6.0	$x_1 = 0,\ y_1 = 0$	**–208.2**	**–230.9**
S_3/P1 [1]	6.1	$x_1 = 0,\ y_1 = 0$	**≤ –336.6**	**≤ –336.6**
CP_S /4	6.0	$x_4 = 0,\ y_4 = 3.7$	**+146.8**	**–77.9**
S_2 /P1 [1]	6.0	$x_1 = 0,\ y_1 = 3.63$	**+135.1**	**–88.3**
CP_S /5	6.0	$x_5 = 3.9,\ y_5 = 0$	**–140.4**	**+51.6**
S_1/P1 [1]	5.9	$x_1 = 4.05,\ y_1 = 0$	**–162.0**	**+106.0**

Table 5: The values of principal residual stress components near statically induced contact dimple in coupons of different thickness.

In work [1], three identical coupons S1, S2, and S3 with a thickness of 4.8 mm were used to determine residual stresses. The thickness of the CP_S sample studied in this work is 6.4 mm. The coordinates of the centers of the probe holes for coupons of both types in the coordinate system, the center of which is located in the center of the contact dimple, are given in Tab. 5. The diameters of the contact dimples are also indicated here. The data from Tab. 5 show that the coordinates of the corresponding holes match well, as do the diameters of the contact dimples that occur with the same indentation force. All these facts mean that ideal conditions exist for assessing the effect of specimen thickness on residual stresses. An increase in thickness leads to a significant decrease in both compressive components of the residual stresses. The principal components of the residual stresses, which relate to the horizontal axis $y = 0$, practically coincide. The principal components of the residual stresses, both compressive σ_1 and tensile σ_2, which are obtained on the vertical axis $x = 0$, decrease by 14 and 51 percent, respectively, with increasing sample thickness.

Information, related to the dynamic indentation of the impactor with hemispherical tip of 20 mm diameter in composite plates of different thickness, is presented in Tab. 6.

Coupon/ Point	Contact dimple diameter. mm	Distance from dimple center to probe hole center x/y, mm	σ_1, MPa	σ_2, MPa
CP_D-20 /6	6.4	$x_6 = 4.2,\ y_6 = 0$	**–26.8**	**+76.8**
D_1/P1 [1]	6.1	$x_1 = 4.05,\ y_1 = 0$	**–82.4**	**+49.0**
CP_D-20 /5	6.4	$x_5 = 0,\ y_5 = 3.8$	**+123.8**	**–40.5**
D_2/P1 [1]	6.1	$x_1 = 0,\ y_1 = 4.05$	**+192.1**	**–58.1**

Table 6: The values of principal residual stress components near dynamically induced contact dimple in coupons of different thickness.

The increase in the diameter of the contact dimple in the CP_D-20 coupon is due to an increase in the impact energy from 40 J to 55 J. The data from Tab. 6 show that, despite the increase in impact energy, the principal residual stress components, defined along the horizontal axis $y = 0$, decrease with increasing coupon thickness.
Information, related to the impact of the indenter with hemispherical tip of 20 mm and 25 mm diameter in composite plates of equal thickness, is presented in Tab. 7.

Coupon/ Point	Contact dimple diameter. mm	Distance from dimple center to probe hole center x/y, mm	σ_1, MPa	σ_2, MPa
CP_D-25 /5	8.4	$x_5 = 4.2,\ y_5 = 0$	**–30.0**	**+124.3**
CP_D-20 /6	6.4	$x_6 = 4.2,\ y_6 = 0$	**–26.8**	**+76.8**
CP_D-25 /6	8.4	$x_6 = 0,\ y_6 = 5.2$	**+191.0**	**+9.1**
CP_D-20 /5	6.4	$x_5 = 0,\ y_5 = 3.8$	**+123.8**	**–40.5**

Table 7: The values of principal residual stress components near contact dimple in coupons after impact by semispherical indenter with different tip diameter.

It is almost impossible to compare the values of residual stresses in the contact dimple centers due to the unreliability of the data obtained for the CP_D-20 coupon. A comparison of the values of the tensile components σ_2 at points located near the intersection of the horizontal axis $y = 0$ and the contour of the contact dimple reveals an increase of 38 percent with an increase in the diameter of the impactor tip from 20 to 25 mm. A similar increase in the value of the tensile component σ_2 at points located near the intersection of the vertical axis $x = 0$ and the contour of the contact dimple is 35 percent.
One of the subjects of the performed research is to identify ways to use the values of residual stresses occurring in the vicinity of the contact dimple to predict the residual strength of damaged composite structures.
A comparison of the data presented in Tab. 5-7 shows an ambiguous effect of changes in both the sample thickness and the impact energy on the residual stress values. This fact indicates the need of further research in this direction. The output of this research should include the results of determining the values of residual stresses obtained for a significant array of coupons of different thickness and stacking sequence for different impact energy levels. However, even at the initial stage, it can be argued that the presence of residual stresses in the vicinity of the contact dimple is a factor that has a significant effect on reducing the residual strength of specimens made of CFRP. This statement is valid both for tensile tests and for stability under the action of compressive loads.
In addition, the values of the residual stress components can be obtained at various stages of cyclic loading of coupons and used as current damage indicators. The evolution of these indicators over the lifetime is an essential link for the quantitative analysis of fatigue damage accumulation inherent in dynamically damaged zone of a composite material. The following section illustrates the realism of this approach.

RESIDUAL STRESS EVOLUTION

The specimen used in this study (CP_S@) is cut from the panel of dimension 320×320×6.4 mm and cross-ply $[0/90]_{9S}$ stacking sequence. It has dimensions 180×30×6.4 mm and the single contact dimple located at the coupon's center. The dimple is caused by static indentation of hardened steel ball of 16 mm diameter with pressing force $P = 3.0$ kN. CP_S@ coupon was subjected to uniaxial push-pull loading with stress range $\Delta\sigma = 318$ MPa and stress ratio: $R = -0.5$ during $N = 1100000$ cycles. After this residual stress components were determined at the centre of contact dimple by the procedure described above. Interference fringe patterns, caused by through hole drilling, are shown in Fig. 16. The quality of interference fringes is quite suitable for reliable quantitative interpretation.
The results of fringe patterns interpretation and the values of principal residual stress components in CP_S@ coupon are listed in the second row of Tab. 8. The third row contains analogous data obtained for CP_S coupon. Comparing σ_2 component values acting along load direction reveals considerable relaxation. Quantitative characteristic of this process consists of [(230.9-48.1)/230.9] = 79.2 per cent. This estimation gives some reason to believe that considered parameter might be used as current damage indicator for deriving an explicit form of damage accumulation function by the approach developed in work [24].

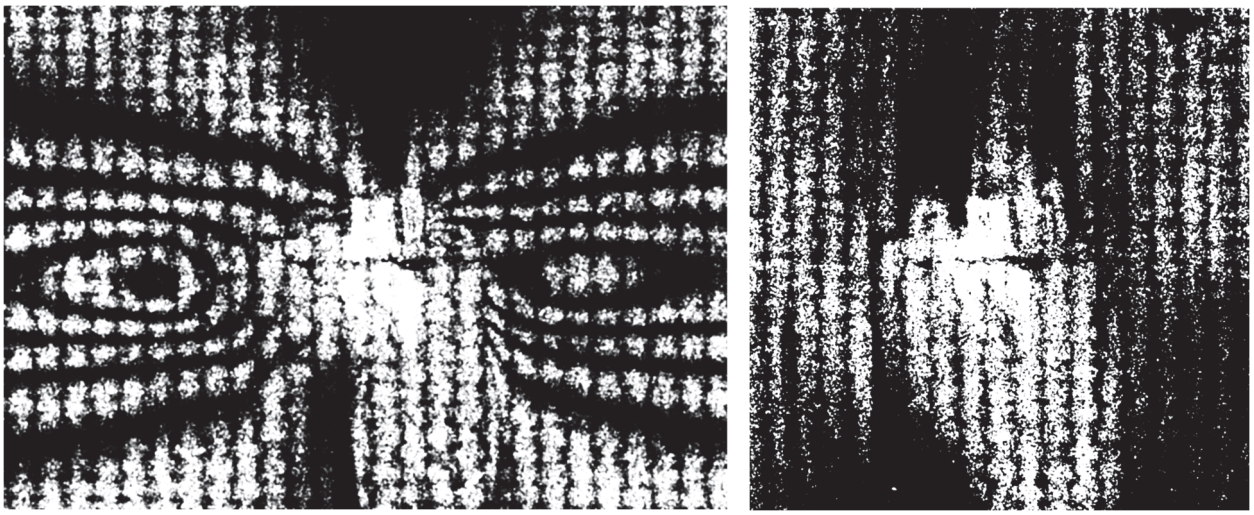

(a) Component u, $\Delta N^{u} = -10.5$ (b) Component v, $\Delta N^{v} = -2.0$

Figure 16: Specimen CP_S@. Interferograms referred to the central point of contact dimple.

Point/ Dimple	Distance from dimple center to probe hole center x/y, mm	ΔN^{u}, fringes	ΔN^{v}, fringes	Δu, μm	Δv, μm	σ_1, MPa	σ_2, MPa
CP_S@/1	$x_1 = 0$, $y_1 = 0$ (center of the dimple and probe hole coincides)	–10.5	–2.0	–3.99	–0.76	**–91.2**	**–48.1**
CP_S/1	$x_1 = 0$, $y_1 = 0$ (center of the dimple and probe hole coincides)	–17.5	–22.0	–6.65	–8.36	**–208.2**	**–230.9**

Table 8: The results of fringe patterns interpretation and values of principal residual stress components at center of contact dimple in CP_S@ and CP_S coupon.

CONCLUSIONS

Novel approach developed in paper [1] has been implemented to determine the principal residual stress components that arise as a result of both static and dynamic contact interaction of a steel spherical indenter and a flat surface of more thick composite plates of the same geometrical dimensions and cross-ply stacking sequence. Availability of significant residual stresses that occur in the zone of contact interaction between the steel spherical indenter and the surface of the composite plate has been established both for static influence and impact. It is shown that high-quality interference fringe patterns and, hence, residual stress values can be reliably obtained by drilling probe holes both inside and outside the boundaries of the contact dimple caused by impact with an energy of 55 J.

The distributions of residual stresses obtained during static and dynamic contact interaction, which leads to the appearance of dimples of almost the same diameter, are compared. A comparison of the values of the principal residual stress components corresponding to the contact interaction of a composite plate with an impactor of different diameters for the same impact energy is presented.

A number of factors have been identified that obviously reduce the residual strength of damaged specimens. In tensile tests, such a factor is the value of the residual tensile component, which occurs at the boundary of the contact dimple located in the horizontal cross-section of the coupon. The value of this component is 15.5% of the ultimate tensile strength of the material. The second parameter, which undoubtedly negatively affects the residual strength, both in tension and compression, is the transition of the component σ_2 sign from "minus" to "plus", which occurs inside the contact dimple. This process is burdened by the presence of a significant stress gradient. The third factor is associated with the occurrence

of a significant negative component of residual stresses in the center of the impact dimple $\sigma_2 = -173.0$ MPa directed along the vertical symmetry axis of the specimen. This is an evident reason of the loss of bearing capacity of dynamically damaged plates during compression tests. It should be borne in mind that this value is significantly "softened" due to the presence of initial tensile residual stress in the coupon $\sigma_2 = +48.6$ MPa.

Evaluation of the influence of coupon's thickness as well as an indentation type and parameters on the results of residual stress determination in the vicinity of contact dimple is presented.

ACKNOWLEDGEMENTS

Authors thank the Russian Science Foundation for providing support in the frame of the 24-19-00117 project (https://rscf.ru/en/project/24-19-00117).

REFERENCES

[1] Eleonsky, S., Pisarev, V. (2025). Residual stresses caused by static and dynamic contact interaction of composite plate and steel spherical indenter, Fracture and Structural Integrity, 71, pp. 246-262. DOI: 10.3221/IGF-ESIS.71.18.

[2] Taheri, H., Hassen, A.A. (2019). Nondestructive ultrasonic inspection of composite materials: a comparative advantage of phased array ultrasonic, Applied Sciences, 9, 1628. DOI: 10.3390/app9081628.

[3] Azad, M.M., Jung, J., Elahi, M.U., Sohail, M., Kumar, P., Kim, H.S. (2024). Failure modes and non-destructive testing techniques for fiber-reinforced polymer composites, J. Mater. Res. Technol., 33, pp. 9519–9537. DOI:10.1016/j.jmrt.2024.11.269.

[4] Tuo, H., Wu, T., Lu, Z., Ma, X. (2021). Evaluation of damage evolution of impacted composite laminates under fatigue loadings by infrared thermography and ultrasonic methods, Polymer Test, 93, 106869. DOI:10.1016/j.polymertesting.2020.106869.

[5] Popow, V., Vogtmann, J., Gurka, M. (2022). In-situ characterization of impact damage in carbon fibre reinforced polymers using infrared thermography, Infrared Phys. & Technol., 122, 104074. DOI:10.1016/j.infrared.2022.104074.

[6] Schwedersky, B.B., de Oliveira, B.C., Albertazzi, A., Flesch, R.C. (2022). Impact damage characterization in CFRP samples with self-organizing maps applied to lock-in thermography and square-pulse shearography images, Expert Syst. with Appl., 192, 116297. DOI: 10.1016/j.eswa.2021.116297.

[7] Berthe, J., Chaibi, S., Portemont, G., Paulmier, P., Laurin, F., Bouvet, C. (2023). High-speed infrared thermography for in-situ damage monitoring during impact test, Compos. Struct., 314, 116934. DOI: 10.1016/j.compstruct.2023.116934.

[8] Zhu, P., Zhang, H., Sfarra, S., Sarasini, F., Usamentiaga, R., Vavilov, V. et al. (2024). Enhancing resistance to low-velocity impact of electrospun-manufactured interlayer-strengthened CFRP by using infrared thermography, NDT and E. Int., 144, 103083. DOI:10.1016/j.ndteint.2024.103083.

[9] Gerdes, L., Walther, F. (2025). Impact damage detection for carbon fiber-reinforced polyurethane by means of active thermography and computed tomography, Engineering Failure Analysis., 170, 109306. DOI:10.1016/j.engfailanal.2025.109306.

[10] Zhou, W., Huang, J., Liu, D. (2021). In situ capture of impact-induced progressive damage and delamination in fiberglass composite laminate with a high-speed optical imaging method. Compos. Struct. 259, 113498. DOI: 10.1016/j.compstruct.2020.113498.

[11] Sasikumar, A., Trias, D., Costa, J., Blanco, N., Orr, J., and Linde, P. (2019). Impact and compression after impact response in the thin laminates of spread-tow woven and noncrimp fabrics, Comp. Struct., 215, pp. 432-445. DOI: 10.1016/j.compstruct.2019.02.054.

[12] Prakash, R., John, M. (2019). Post-impact fatigue damage analysis of quasi-isotropic CFRP laminates through infrared thermography, Frattura ed Integrità Strutturale, 49, pp. 536-546. DOI: 10.3221/IGF-ESIS.49.50.

[13] Kotter, B., Endres, J., Korbelin, J., Bittner, F., Endres, H-J., Fiedler, B. (2021). Fatigue and fatigue after impact behaviour of thin- and thick-ply composites observed by computed tomography, Compos Part C: Open Access, 5, 100139, DOI: 10.1016/j.jcomc.2021.100139.

[14] Kravchenko, S.G., Volle, C., Kravchenko, O.G. (2021). An experimental investigation on low-velocity impact response and compression after impact of a stochastic, discontinuous prepreg tape composite, Compos Part A: Appl. Sci. and Manuf., 149, 106524. DOI: 10.1016/j.compositesa.2021.106524.

[15] Gerdes, L., Richle, S., Mrzljak, S., Hülsbusch, D., Barandun, G., Walther, F. (2022). Computed tomography-based characterization of impact and fatigue after impact behavior of carbon fiber-reinforced polyurethane. Compos. Struct., 289, 115474. DOI: 10.1016/j.compstruct.2022.115474.

[16] Gohel, G., Bhudolia, S.K., Leong, K.F., Gerard, P. (2023). Understanding the impact properties and damage phenomenon of ultra-lightweight all-thermoplastic composite structures. Int. J. Impact. Eng., 172, 104405. DOI: 10.1016/j.ijimpeng.2022.104405.

[17] Bin, L., Wei, W., Leigh, S. (2023). Experimental and numerical response and failure of laterally impacted carbon/glass fibre-reinforced hybrid composite laminates, Int. J. Impact. Eng. 179, 104654. DOI: 10.1016/j.ijimpeng.2022.104654.

[18] Reiner, J., Fu, Y.-F. (2022). Data-driven parameter identification to simulate progressive damage in fiber reinforced laminates under low velocity impact, Int. J. Impact. Eng., 180, 104711. DOI: 10.1016/j.ijimpeng.2022.104711.

[19] Qiao, Z., Zhefeng ,Y. (2024). A modified spring-mass model of low-velocity-impact on composite laminate including shearing deformation at delaminated region and reduction on membrane stiffness, Int. J. Impact. Eng., 185, 104847. DOI: 10.1016/j.ijimpeng.2022.104847.

[20] Pisarev, V.S., Eleonsky, S.I., Chernov, A.V. (2015). Residual stress determination in orthotropic composites by displacement measurements near through hole, Experimental Mechanics, 55, pp. 1225–1238. DOI:10.1007/s11340-015-0015-3.

[21] Eleonsky, S., Kazantsev, D., Pisarev, V., Statnik, E. (2023). Influence of plate thickness on the results of residual stresses determination by through hole drilling in orthotropic composites of different fiber orientation, Materials Today: Proceedings. DOI:10.1016/j.matpr.2023.09.072.

[22] Rastogi, P. (2001). Digital speckle pattern interferometry and related techniques. West Sussex: Wiley.

[23] Eleonsky, S., Pisarev, V., Statnik, ES., Salimon, A.I., Korsunsky, A.M. (2024). Residual stress determination by blind hole drilling and local displacement mapping in aluminium alloy aerospace components, Frattura ed Integrita Strutturale, 69, pp. 192-209. DOI:10.3221/IGF-ESIS.69.14.

[24] Matvienko, Yu.G., Pisarev, V.S., Eleonsky, S.I. (2021). Evolution of fracture mechanics parameters relevant to narrow notch increment as a measure of fatigue damage accumulation, International Journal of Fatigue, 149, 106310. DOI: 10.1016/j.ijfatigue.2021.106310.